Pergamon

0956-7151(93)E0033-Y

Acta metall. mater. Vol. 42, No. 4, pp. 1155–1162, 1994

0956-7151/94 $6.00 + 0.00

METAL–CERAMIC INTERFACES IN LASER COATED ALUMINIUM ALLOYS

X. B. ZHOU and J. Th. M. De HOSSON

Department of Applied Physics, University of Groningen, Zernike Complex, Nijenborgh 4, 9747AG Groningen, The Netherlands

(Received 22 September 1993)

Abstract—A novel process was developed to firmly coat an aluminium alloy, Al6061, with α-Al_2O_3 by means of laser processing. In this approach a mixture of SiO_2 and Al powder was used to inject in the laser melted surface of aluminium. A reaction product α-Al_2O_3 layer of a thickness of 100 μm was created which was well bonded to the aluminium surface.

Various interfaces, Al/α-Al_2O_3, Al/mullite and α-Al_2O_3/mullite, were studied by conventional transmission electron microscopy (CTEM) and high resolution electron microscope (HREM). It turns out that the presence of the Al/mullite interface may be essential to form a well bonded oxide layer and the high Si-content α-Al_2O_3 intermediate layer may be wetted better by liquid Al. Investigations of the interface structures and wetting phenomena during laser processing are presented and a simple correlation between wetting phenomena and interface strength is derived.

1. INTRODUCTION

The low hardness and poor wear resistance are the principal reasons that limit the potential applications of aluminium alloys. Hardfacing on aluminium alloys, e.g. by electro-deposition and anodizing, may improve the hardness and wear resistance significantly. However, there are still major drawbacks in these conventional methods. The bonding between these coatings and aluminium alloys is usually weak [1–3] and may cause failure during application. The amorphous anodizing layer [3] is brittle with a relative low hardness ($HV_{0.1}$ 250–500) to resist abrasive wear. Recently a few attempts were made using a laser to coat an intermetallic or a ceramic layer on the surface of aluminium alloys [4, 5]. However there are several difficulties in this process.

First, the high melting point of ceramics which is close to the boiling point of aluminium requires a high energy density of the laser beam to melt ceramic coating. It will generate a strong convective flow in the aluminium melt pool, and eventually it may lead to a substantial surface roughness and destroy the ceramic coating. Secondly, the large difference of thermal expansion coefficient between aluminium (about 22 μm/m°C) and ceramics (mostly below 8 μm/m°C) will introduce high stresses at the metal/ceramics interface during rapid cooling which may cause the interface bonding to fail. Finally, the wetting of aluminium on most ceramics is usually poor and the rapid melting and solidification of laser process require a good wetting between liquid metal and solid ceramic within a very short period, say from 0.01 to 0.1 s. Therefore it was pointed out [4] that laser coating on aluminium alloys is very difficult compared with coatings on other metals such as iron-base materials [6, 7]. In order to overcome these drawbacks, we have developed a novel process by means of a chemical reaction. Preliminary results and ideas were presented in [8]. In this reaction coating, a mixture of SiO_2 powder with aluminium was used to inject in the laser melted surface of aluminium. The following reaction occurred $2Al + 3/2SiO_2 = Al_2O_3 + 3/2Si$. A large amount of heat will release from this exothermic reaction. For instance, if the reaction occurs at 1173 K the exothermic heat is 383.4 kJ/g · mol which is sufficient to melt the reaction products. Therefore a much lower laser energy density (about one fourth as before) is required, and consequently the convective flow inside the melt pool can be significantly reduced. This will diminish the roughness of the coating on Al. The large, negative value of the free energy (−297.7 kJ/g · mol at 1173 K) in this reaction may also provide a rapid wetting between the oxide and the metal substrate. The reaction product of α-Al_2O_3 layer of a thickness of 100 μm was created on the aluminium alloy surface by this reaction coating technique [8]. It turns out that the reaction layer was well bonded to the aluminium surface. The micro-hardness of the layer exhibited a very high value around $HV_{0.2}$ 2300–3060 and a wear test demonstrated that there was no detectable wear from the coating.

In this study we present a more detailed investigation of the interface structures and wetting process during this novel reaction coating process, applying mainly conventional transmission electron microscopy (HREM).

2. EXPERIMENTS

Because of the low melting point of the Al substrate, a relatively high laser scan velocity and low energy density of beam were used in order to reduce the roughness of the oxide layer. The laser parameters (CW-CO_2 Spectra Physics 820) were: output power of 1.0–1.2 kW, scan velocity of 40 mm/s and defocus of 20 mm with a beam diameter of 3 mm. An overlap of subsequent laser tracks of 67% was applied in order to form a sufficiently thick layer. A mixture of SiO_2 and Al powder with a mole ratio of 1:1 was injected into the laser melt pool of the Al6061 substrate. The chemical composition of Al6061 is 1.0 wt%Mg, 0.6 wt%Si, 0.25 wt%Cu, 0.25 wt%Cr. The particle sizes of the powder ranged from 5 to 45 μm in the case of Al powder and from 2 to 40 μm for SiO_2. A relatively smaller size of particulates is favourable for a homogeneous reaction, although, because of aggregation of small SiO_2 particles with aluminium, it becomes more difficult to feed the mixing powder through the home-made powder feeding system.

A JEM-200CX transmission electron microscope operating at 200 kV was used to study the microstructure and interfaces. Further, a high resolution electron microscope (HREM) (JEM-4000EX II) with point-to-point resolution of 0.17 nm resolution operating at 400 kV was applied. The specimen for both TEM and HREM were cross sectioned and glued together afterwards. Subsequently, the sample was ground to about 60 μm and dimpled later on to about 15 μm near the centre. Ion milling was used for the final thinning. Simulation of HREM images was carried out using the EMS program [9] to compare the experimental images with the simulated images. In the simulations a specimen thickness was chosen to be 10 nm, an aperture diameter of 20 nm^{-1}, a spherical aberration constant of $C_s = 1.0$ mm, a spread of focus of $\delta = 11$ nm and a beam semi-convergence $\alpha_g = 0.7$ mrad.

X-ray diffraction indicated [8] that α-Al_2O_3 was the predominant major phase in the reaction layer. Further, silicon and mullite, crystalline SiO_2 co-exist. The silicon concentration in the α-Al_2O_3 layer is very low about 0.17–3.2 mol% as analysed by EDS (Energy Dispersive Spectrometry) in the scanning electron microscope (SEM). According to SEM and EDS analyses, two interface layers usually exist between the reaction α-Al_2O_3 coating and the aluminium substrate as depicted in Fig. 1(a): one is the high silicon content layer bound to the α-Al_2O_3 coating and another is a thin layer with a high Al-content in contact with the aluminium substrate. Based on the TEM observation, the structure in the high silicon content layer consists mainly of a mullite phase and an amorphous silicate phase. The thin oxide layer located between the silicate and the aluminium substrate is α-Al_2O_3 with a relative high Si content (4–6 mol%). As the α-Al_2O_3 interface layer is very thin, quite often an Al/mullite interface is created as shown in Fig. 1(b). According to SEM observations, mullite is always firmly bonded to Al. However pores or debonding between Al/α-Al_2O_3 interface is sometimes observed. In particular when the interface consists only of α-Al_2O_3 coating/aluminium substrate without the two interlayers, failure occurs frequently as displayed in Fig. 1(c).

Figure 2 represents a TEM bright field image of Al/Al_2O_3 interface, where a crystallographic orientation relationship $[2\bar{2}1]_{Al2O3}//[110]_{Al}$ and $(110)_{Al2O3}//(\bar{1}11)_{Al}$ exists. Figure 3 illustrates an interface between the mullite layer and the Al substrate, whereas the mullite/α-Al_2O_3 interface is depicted in Fig. 4. Here the bonding between the metal/oxide and

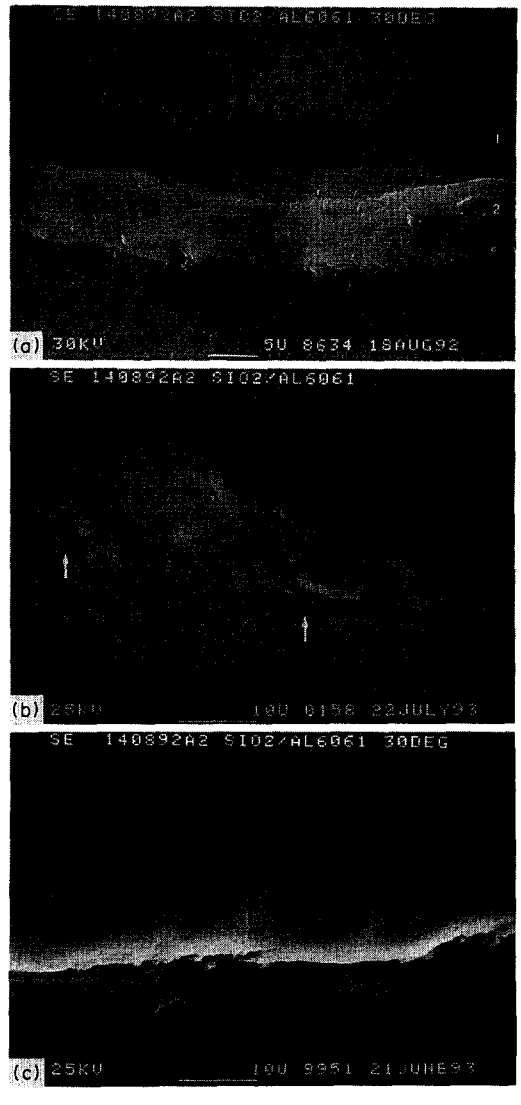

Fig. 1. SEM picture from a cross-section of the reaction coating indicates: (a) two intermediate layers, a high Si-content oxide (1) and a high Al-content oxide (2) between the α-Al_2O_3 coating and Al substrate. (b) Pores existing between α-Al_2O_3 thin reaction layer and Al substrate. (c) Debonding between α-Al_2O_3 reaction coating and Al substrate without intermediate layers.

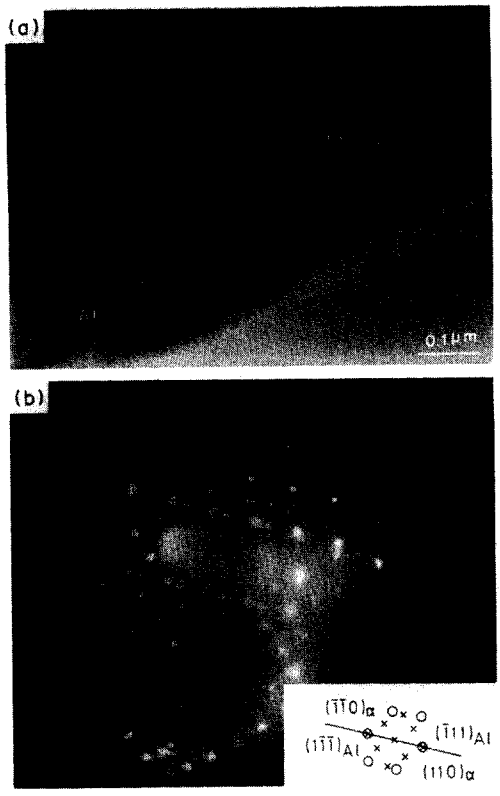

Fig. 2. (a) TEM bright field image of Al_2O_3/Al interface and (b) diffraction pattern indicating $[2\bar{2}1]_{Al2O3}//[110]_{Al}$ and $(110)_{Al2O3}//(\bar{1}11)_{Al}$; ○ belongs to Al, × belongs to Al_2O_3.

Fig. 3. TEM micrograph illustrates the mullite/Al substrate interface substrate.

Fig. 4. TEM image of mullite/Al_2O_3 interface.

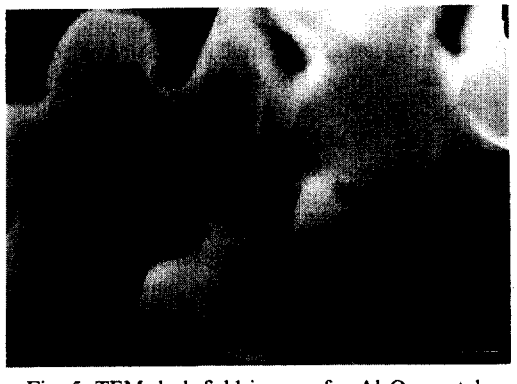

Fig. 5. TEM dark field image of α-Al_2O_3 crystals.

oxide/oxide are good. Figure 5 represents a typical TEM micrographs of α-Al_2O_3 grains inside the reaction coating. The grain size of the α-Al_2O_3 ranged from 1 to 3 μm. Figure 6 shows the mullite cubes and plates in the coating. The sizes of the mullite cubes and the width of the mullite plates are very small, ranging between 0.1 and 0.2 μm. The mullite cube planes are on {110} and the growth direction of the mullite plate is on ⟨100⟩. The facet of mullite cube on the {110} represents the fact that the {110} is the lowest energy plane.

Figure 7 illustrates HREM images of mullite viewed along the [010] direction. By comparison with the simulated images (Fig. 8), where the 3:2 mullite ($3Al_2O_3 \cdot 2SiO_2$) [10] was used, the defocus depths of the HREM image can be resolved. At a defocus of −72, a shift of columns of atoms, which is randomly distributed over the structure, can be observed in the HREM image. This shift of atoms is caused by the presence of point defects in the mullite lattice. In Fig. 9 a HREM image of silicon precipitate is depicted as observed along the [110] direction. Clearly, (111) twins and stacking faults have been developed. These twins and stacking defects indicate that the silicon precipitate is highly strained. Because a crystallographic orientation relationship between aluminium and mullite is hard to observe, an image at atomic resolution on both side of metal/oxide interface could not be obtained. Figure 10 represents an example of a HREM image of an Al[110]/mullite interface.

3. DISCUSSION

During laser processing of a ceramic coating onto metals the interface strength between the ceramic layer and the metallic substrate as well as the wetting phenomena are the two predominant factors. Usually enhanced wetting induces improved strength of the interface and therefore it is appropriate to find a

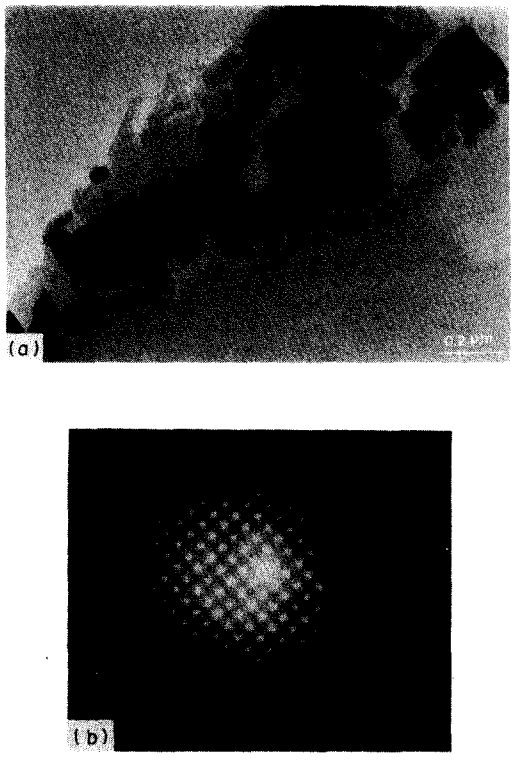

Fig. 6. (a) TEM bright field image of mullite cubes and plates and (b) diffraction pattern.

relationship between wetting phenomena and interface strength. In general a metal/ceramic interface can be categorised as a reactive interface and non-reactive interface, where the free energy between the metal and ceramic is negative or positive, respectively. Chemical reactions can provide a rapid and complete wetting process and may benefit the formation of the oxide coating on metal by laser processing. According to thermodynamic calculations of the reaction between Al and SiO_2 [8], a large (negative) free energy of -297 KJ/g · mol at 1173 K, would significantly improve the wetting of metal onto oxide. However as the coating was produced by overlapping laser tracks, the negative free energy of the second laser track would not contribute to the wetting of the edge of the first laser track where the reaction has already occurred. Therefore, in this case the wetting and interface strength of a non-reactive metal/ceramic interface could be more relevant. However, still chemical bonds could be formed locally along this interface as a result of which the work of adhesion is affected, i.e. the strength of the interface.

There are mainly two different interactions that may contribute to the work of adhesion between a metal and a ceramic, i.e. physical and chemical interactions. Here the work of adhesion or, as it is also called, the interfacial free energy of adhesion, W_{ad} is taken as the energy required to separate a plane of metal (m) from a plane of ceramic material (c), from their equilibrium distance R to infinity, i.e.

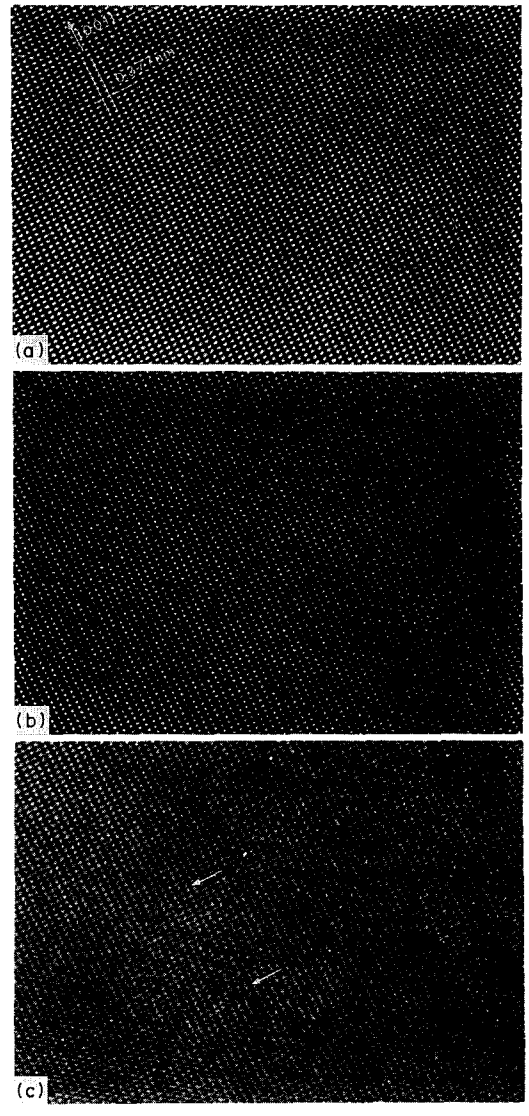

Fig. 7. HREM images of mullite on [010] with a series of defocus values: (a) -24; (b) -48; (c) -72.

described by the interaction between two semi-infinite bodies

$$W_{ad} = -\int_R^\infty f_{ad,mc}\,dz \tag{1}$$

where the force is given by

$$f_{ad,mc} = 2\pi N_m N_c \int_z^\infty dp \int_p^\infty q\,dq \int_q^\infty g(r)\left[-\frac{du}{dr}\right]dr \tag{2}$$

$u(r)$ represents the interaction potential, N is the atomic density [m^{-3}] and $g(r)$ is the probability of finding an atom at a distance r of a given one. The last integral gives the interaction between a metal atom and a slab of the ceramic material. The integral over q gives the interaction between a metal atom and the complete ceramic materials, whereas a subsequent integration over p yields the total interaction between the whole metal and whole ceramic material. The

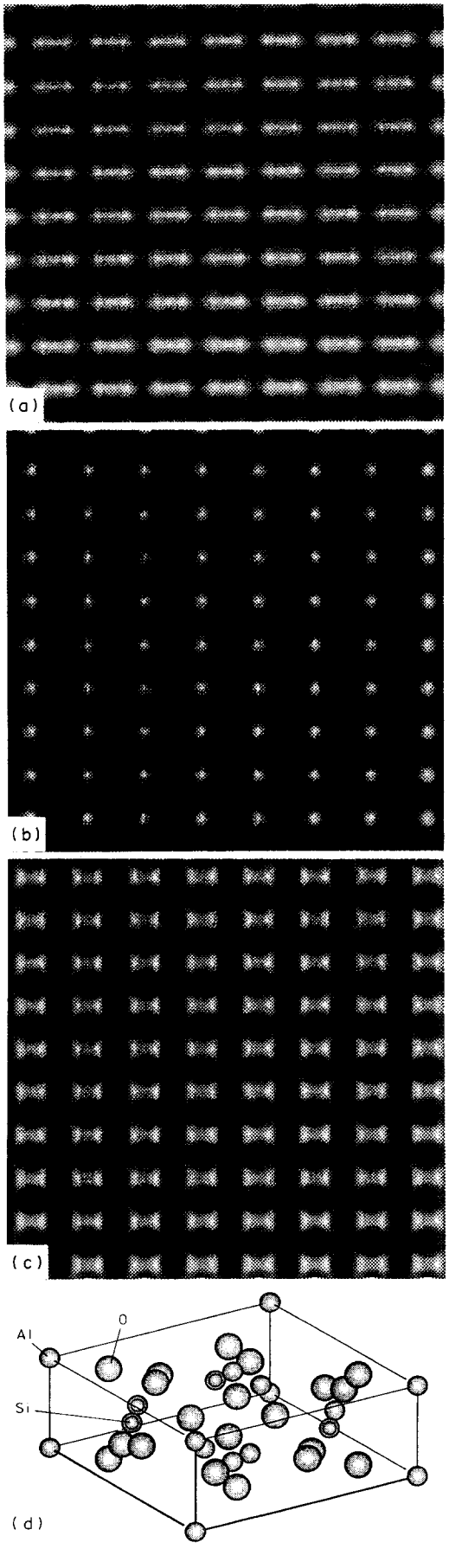

Fig. 8. Simulated HREM images of mullite structure (d) at the same defocus values as in Fig. 7: (a) −24; (b) −48; (c) −72.

Fig. 9. HREM image of Si precipitate on [110] showing (111) twins and stacking defects.

Fig. 10. HREM image of Al[110]/mullite interface.

interaction potential $u(r)$ is commonly described by the London–dispersion interactions, i.e. the attraction between an instantaneous dipole and its induced dipole: i.e. $-A/r^6$, where $A = 3\,\alpha_m\alpha_c I_m I_c/2(I_m + I_c)$; I_m, I_c are the ionisation potentials of the two atoms and α_i represent their polarizabilities. Substitution of this dispersion force in equation (2), while $g(r)$ is set equal to 1, gives a contribution due to the physical interaction to W_{ad} as written in the first part of the following equation

$$W_{ad} = n_m n_c \pi \frac{\alpha_m \alpha_c}{8R^4}\left(\frac{I_m I_c}{I_m + I_c}\right) - \frac{\beta}{2B}\Delta F_{mc} \qquad (3)$$

where n is the number of atoms per unit surface area of the interface. The second term in equation (3) represents the contribution due to chemical interactions: $1/2\ \Delta F_{mc}$ is the standard free energy of ionic bonds, β is the density of the ionically bonded sites and B is the number of bonds in a gram mole. In most metal/oxide interface of engineering interest, the first part describing the physical interaction in equation (2) is relative weak [11], whereas the second part due to the chemical interaction is more predominant. Several observations indicated [11–16] that a chemical bond was built up between

metal/oxide interface, as suggested in equation (3). However, the detailed understanding of the interface structure is still very complex for each individual case. For the sake of simplicity, we assume that the bonding of metal/oxide interface has a similar structure as in the most stable oxide structure of the metal. This interface is also the weakest part in the system compared to the cohesive energy of ceramic. Consequently the elastic modulus across the interface and the interface spacing may be approximately represented by the values of the metal oxide. A theoretical tensile strength, assuming cleavage fracture and no plasticity, between a perfectly bonded metal/oxide interface might be estimated assuming that the increase in interface energy associated with the creation of new surface areas is equal to the work of adhesion at room temperature. It is assumed that the interface is intrinsically brittle, i.e.

$$\sigma_{th} = \sqrt{\frac{W_{ad} E_{m0}}{2R}}. \tag{4}$$

Introduction of equations (3) into (4) and neglecting the physical interaction term, the theoretical tensile strength for cleavage fracture is given by

$$\sigma_{th} = \sqrt{-\frac{\beta \Delta F_{m0} E_{m0}}{4RB}} \tag{5}$$

where E_{m0} is the elastic modulus of the metal/ceramic and R is the spacing between two strong chemical bond at the interface. Equation (5) suggests that the interface strength is enhanced by a strong chemical bond over the interface, e.g. higher values of $-\Delta F_{m0}$ and E_{m0}, together with an increase of β. HREM studies [14–18] of the metal/oxide interface suggest that the interface spacing is comparable in magnitude to the atomic spacing. However the elastic modulus in equation (5) is likely to be overestimated because the interface bond might be relatively weaker than the bond of the most stable metal oxide, and the geometry at the interface may be completely different from the metal oxide. In the other words, the probability of a strong bond which can be built up across the interface is relatively less comparing to the pure metal oxide crystal. Therefore a detailed study of atomic arrangement at an interface is necessary.

It is known that the work of adhesion between a liquid metal and a solid can be described by $W_{ad} = \gamma_{sv} + \gamma_{lv} - \gamma_{sl}$ (Dupré's equation) where γ represents the interfacial free energy (s: oxide, l: liquid metal, v: vapour). Dupré's equation can be rewritten as $\gamma_l(1 + \cos\theta)$ (Young's equation). Here, the spreading pressure is neglected that denotes the difference between γ_s, the surface free energy of the bare solid surface, and γ_{sv}, the surface free energy of the solid in the presence of saturated vapour from the liquid metal (i.e. no extra adsorbed layer). The work of adhesion does not change significantly from high temperature to room temperature. Introduction of the expression of W_{ad} at high temperature into equation (4) gives

$$\sigma_{th} = \sqrt{\frac{\gamma_l(1 + \cos\theta) E_{m0}}{2R}}. \tag{6}$$

In fact it is interesting to note that experimentally the initiation fracture resistance in a model system of gold of thickness h bonded to sapphire, appears to follow $W_{ad}[1 + \sigma_0 h / W_{ad}]^{1/2}$, where σ_0 represents the uniaxial yield stress of gold [19].

From equation (6) it can be clearly seen that a small contact angle θ and a strong interaction, e.g. larger E_{m0}, between metal and oxygen will increase the theoretical strength. Table 1 lists some of the calculated results of σ_{th} which ranges from 1 to 40 GPa. These are much higher than the values of metal/ceramic interfaces of any kind of joining or coating in real practice which lie in the order of 10^1–10^2 MPa [20]. This is only partly because of the overestimate of the elastic modulus at the interface, since in real practice primarily the mode of deformation, the existence of interface defects and interface residual stress determine the interface strength. In particular the zone around an interface crack on the metal side that contains a distribution of lattice dislocations may affect considerably the stress level to be built up for rupture along the interface [21].

Following the Griffith–Orowan analysis, suppose that there is a crack of length $2c$ existing along the metal/ceramic interface and the radius of curvature at the tip of the crack is ρ, then the nominally applied stress can be related to the maximum stress at the crack tip approximately by $\sigma_{max}[\rho/4c]^{1/2}$. We may reasonably assume that fracture will occur when σ_{max} equals σ_{th} [equation (6)], i.e. the fracture strength of

Table 1. Interface strength of various metal/oxide interface. The data were taken from [22, 32] and calculated according to equations (6) and (7)

Oxides	Metals	T (°K)	θ°	E_{m0} (GPa)	γ_l (J/m^2)	R_{m0} (nm)	σ_{th} (GPa)	σ_{inf} (0.1 μm) (MPa)
Al_2O_3	Al	1213	170	380	0.86	0.183	3.7	78.8
	Al	1523	48	380	0.86	0.183	38.8	825.4
	Fe	1823	141	1.18	1.86	0.206	1.1	24.7
	Si	1723	80	72.3	0.73	0.174	13.3	278.3
Cr_2O_3	Fe	1823	88	1.18	1.86	0.206	2.3	53.3
MgO	Fe	1823	130	1.18	1.86	0.206	1.4	31.3
	Si	1723	101	72.3	0.73	0.174	11.1	231.1
ZrO_2	Fe	1808	111	1.18	1.86	0.206	18.5	83.5
	Si	1723	71	72.3	0.73	0.174	14.2	295.7

the interface is approximated by

$$\sigma_{\inf} \cong \sqrt{\frac{\gamma_l(1+\cos\theta)E_{m0}\rho}{8cR}}. \quad (7)$$

Equation (7) gives a simple correlation between the interface strength and the wetting angle as well as the geometry of the interface crack ρ/c. Suppose the interface fails by a brittle fracture then ρ is still approximately equal to R and the interface strength may be calculated from equation (7) for various crack lengths. In Table 1 the results for $2c = 0.1\,\mu$m are listed. It is clearly seen that these values provide a more realistic estimate of practical interface strength. In fact during the coating or joining processes, interface cracks may be introduced by non-wetting. Therefore according to equation (7), a smooth surface and a good wetting will be expected to improve the interface strength significantly. However, pores filled with gas at a metal/ceramic interface may not behave as a crack at the interface as the curvature of pores is much large than the dimension of a interface spacing. In our reaction coating pores can be observed quite often along the Al–α-Al_2O_3 interface but the complete interface are still bonded.

In a laser melt pool, the temperature at the centre of laser melt pool is very high, but the temperature at the side of melt pool is relatively low, i.e. about the melting point of Al. Therefore the wetting near the edge would be dominated by the contact between reaction product of α-Al_2O_3 or mullite and liquid Al at the melting point. It is known that the wetting of α-Al_2O_3 by liquid Al is rather temperature-dependent. For instance the wetting angle of Al to α-Al_2O_3 [22] decreases from 170 at 1213 K to 48 at 1523 K. Then the reaction product of α-Al_2O_3 in the first laser track might not be wetted by liquid aluminium from the second track because of the lower temperature. As a consequence debonding can be sometimes observed along the Al/Al_2O_3 interface.

Further, wetting can be improved by a nonstoichiometric composition. For instance, the wetting angle decreases from 116 to 84° for Cu/UO_2 when the O/U ratio increased from 2.001 to 2.084 [23], and decreases from 120 to 0° for Cu/TiC when Ti/C ratio decreased from 1 to 0.5. It is known that mullite [10] is a nonstoichiometric silicate compound with a chemical composition variation over a wide ranging from $3Al_2O_2 \cdot 2SiO_2$ to $2Al_2O_3 \cdot SiO_2$. One important feature of mullite is that there are many oxygen vacancies present which are always accompanied by the occupation of tetrahedral Al sites and a shift of the neighbouring O atoms [24]. This kind of oxygen vacancy and Al occupation may favour the diffusion of Al through the oxide. Similarly, the wetting of α-Al_2O_3 by liquid Al can also be improved by the presence of Si or SiO_2 in Al_2O_3. It is known that there is an incubation period preceding wetting which was observed in every wetting process. A small percentage of SiO_2 (0.1–3%) added to Al_2O_3 may significantly decrease the incubation period [25]. Therefore the wetting of liquid Al on mullite and a high Si-content Al_2O_3 is better compared to pure Al_2O_3.

In addition, the adhesive strength of the interface is also effected by point defects existing in an oxide. Because of an extreme discontinuity in the dielectric properties across the metal–ceramic interface, the charged ions and defects in the ceramic may gain stability by proximity to the highly polarizable metal. From classical electrostatics this stabilisation energy is given by [26]

$$U(R) = \xi \frac{Q^2}{4R\epsilon_c} \frac{\epsilon_c - \epsilon_m}{\epsilon_c + \epsilon_m}, \quad (8)$$

where ξ is added here to represented the defect density, Q is the defect charge, R the interface spacing, ϵ_m and ϵ_c are the dielectric constants of metal and ceramic, respectively. According to equation (8), the bond strength between the ceramic and the metal is enhanced by highly charged defects at a high density. Therefore the point defects in mullite identified by HREM may be favourable to the interface strength. Because of the screening effects due to the highly polarizable metal segregation enthalpies of charged defects to the interface might be much larger than the corresponding segregation enthalpies to free surfaces of the ceramic material which is generally speaking in contrast to the situation in metals [27]. As a consequence the defects in ceramic/metal systems may act as cohesion enhancers since in that case the interface energy will be enhanced. However, at this point it has to be emphasized that the formulation of the binding between metal/ceramic interfaces by (classical) image interactions is just an alternative way of describing the chemical binding term $-\Delta F_{mc}$ [equation (3)] and not an additional effect [28].

An additional reason for a good adhesion between aluminium and mullite is a smaller lattice misfit compared the Al/α-Al_2O_3, provided a favourable orientation relationship exists. For instance, the lattice misfit of mullite/Al on the plane of mullite(120)/Al(110) is 0.73% in the direction of mullite[001]/Al[110] and 4.37% in the direction of mullite[210]/Al[001], but the misfit on the plane of Al_2O_3(001)/Al(111) is 16.7% in the direction of Al_2O_3[100]/Al[110]. In this way the number β of atom pairs expressed in equations (3) and (5) at the interface Al/mullite may be larger than that of Al/Al_2O_3, and a higher adhesion will be achieved. Further, a smaller lattice misfit may also lead to a smaller effective interface separation that in its turn contributes to a larger stabilisation energy based on classical electrostatics [equation (8)].

Beside a good adhesion between mullite and Al, the mechanical properties of mullite are very attractive as well. Since mullite is not subject to any polymorphic conversion or volume change, it exhibits a high thermal shock resistance [29]. It was reported [30] that a reaction-bonded mullite ceramics exhibits high

fracture strength (290 MPa) and the volume expansion of the reaction almost compensates for the shrinkage upon sintering. This superior ability of mullite to resist deformation [16] at high temperature prevents cracking along the interface. Therefore the formation of a mullite interface layer may be crucial to create a well bonded oxide coating on Al alloys in such a laser coating process for engineering applications.

In order to form a mullite structure, a lower fraction of Al in the mixture powder of SiO_2 and Al may be used during the reaction coating. In the molten layer of oxide, the silicon is over-saturated and will diffuse into the aluminium substrate through the metal/oxide interface. Therefore the silicon concentration at the metal/oxide interface will be rather high which favours the formation of mullite composition ranging from $3Al_2O_3 \cdot 2SiO_2$ to $2Al_2O_3 \cdot SiO_2$, according to the equilibrium phase diagram in Al_2O_3–SiO_2 system [31]. Similar results have been reported [16] in a glazing processing on aluminium with silicate, where mullite crystals developed at the interface between porcelain and aluminium fired at high temperature.

4. CONCLUSIONS

Two types of interface layers, namely mullite and a high Si-content Al_2O_3, have been identified between the α-Al_2O_3 reaction coating and Al6061 substrate. The interface bonding of mullite/Al is always good but pores and debonding between α-Al_2O_3 and Al are sometimes observed. Point defects in the mullite crystal were resolved by a series of defocus of HREM images combined with image simulations. Twins and stacking defects in Si precipitates in the coating were observed with HREM. An approximate expression that relates interface strength to wetting properties was investigated for a metal/ceramic interface. It is figured out that a good wetting can not only improve the theoretical strength of a perfect interface but also reduce the possibility of crack formation along the interface which determine the practical interface strength. In this reaction coating the wetting process is mainly governed by the contact of liquid Al with the reaction products of mullite and α-Al_2O_3. The non-stoichiometric behaviour and point defects in the mullite may be contributed to a good wetting behaviour with Al and adhesive strength. The formation of mullite/Al interface may be essential to form a good bond by reaction coating on Al alloy, and a high Si-content Al_2O_3 interface layer may be wetted better than pure α-Al_2O_3 by liquid Al.

Acknowledgements—This work is part of the research program of IOP-Metalen (C91-513-RG-TN), The Hague, The Netherlands and of the Foundation for Fundamental Research on Matter (FOM-Utrecht) and has been made possible by financial support from the Netherlands Organisation for Research (NWO-The Hague) and The Netherlands Foundation for Technical Sciences (STW-Utrecht).

REFERENCES

1. F. J. Monterio, M. A. Barbosa, D. H. Ross and D. R. Gabe, *Surf. Inter. Analy.* **17,** 519 (1991).
2. D. Pantelis, A. Houndri, S. Polymenis and Y. Chryssoulakis, *J. Physique, Coll. C7, Suppl.* **1,** C7–111 (1991).
3. P. Hedenqvist and A. Roos, *Surf. Coat. Technol.* **48,** 41 (1991).
4. M. Pilloz, J. M. Pelletier, A. B. Vannes and A. Bignonnet, *J. Physique, Coll. C7 Suppl.* **1,** C7–117 (1991).
5. H. J. Hegge, J. Boetje and J. Th. M. De Hosson, *J. Mater. Sci.* **25,** 2335 (1990).
6. X. B. Zhou and J. Th. M. De Hosson, *Acta metall. mater.* **39,** 2267 (1991).
7. J. Th. M. De Hosson, X. B. Zhou and M. van den Burg, *Acta metall. mater.* **40,** S139 (1992).
8. X. B. Zhou and J. Th. M. De Hosson, *Scripta metall. mater.* **34,** 55 (1993).
9. P. Stadelmann, I²M-EPFL, CH-1015 Lausanne, Switzerland.
10. S. Hamid Rahman and H.-T. Weichert, *Acta crystallogr.* **B46,** 139 (1990).
11. F. Delannay, L. Froyen and A. Deruyffere, *J. Mater. Sci.* **22,** 1 (1987).
12. E. Gillet, B. Ealet and J. L. Berlioz, *Surf. Intf. Analyt.* **16,** 461 (1990).
13. K. H. Johnson and S. V. Pepper, *J. appl. Phys.* **53,** 6634 (1982).
14. M. D. Keeffe, *J. Mater. Res.* **6,** 2371 (1991).
15. J. F. Knott, *Fundamentals of Fracture Mechanics.* Butterworths, London (1973).
16. W. D. Kingery, *Introduction to Ceramics*, pp. 116, 436, 605. Wiley, New York (1967, 1960).
17. A. Bourret, *J. Physique Coll. C7, Suppl.* **51,** C1–13 (1990).
18. Y. Ishida, *J. Physique Coll. C7, Suppl.* **51,** C1–13 (1990).
19. I. E. Reimanis, B. J. Dalgleish and A. G. Evans, *Acta metall. mater.* **39,** 3133 (1991).
20. J. T. Klomp, *Surface and Interfaces of Ceramics Materials* (edited by L.-C. Dufour *et al.*), p. 375. Kluwer Academic (1989).
21. A. G. Evans and B. J. Dalgleish, *Acta metall. mater.* **40,** S295 (1992).
22. G. V. Samsonov, *The Oxide Handbook*, pp. 224, 452. IFI/Plenum, New York (1973).
23. M. G. Nicholas, *Surface and Interfaces of Ceramic Materials* (edited by L.-C. Dufour *et al.*), p. 393. Kluwer Academic (1989).
24. C. Paulmann, S. H. Rahman and H. T. Weichert, *Electron Microsc.* **2,** 445 (1992).
25. T. Choh and T. Oki, *J. Japan. Inst. Metals* **12,** 1209 (1987).
26. A. M. Stoneham and P. W. Tasker, *Mater. Sci. Res.* **21,** 155 (1986).
27. J. R. Rice, *Chemistry and Physics of Fracture* (edited by R. M. Latanision and R. H. Jones), p. 23. Martinus Nijhoff, The Netherlands (1987).
28. M. W. Finnis, *Acta metall. mater.* **40,** S25 (1992).
29. J. Hlavac, *The Technology of Glass and Ceramics: An Introduction*, p. 40. Elsevier, Amsterdam (1983).
30. Suxing Wu and N. Clausses, *J. Am. Ceram. Soc.* **74,** 2448 (1991).
31. E. M. Levin, C. R. Robbins and H. F. Mcmurdie, *Phase Diagrams for Ceramist*, p. 123. American Ceramic Society, Ohio (1964).
32. *Handbook of Chemistry and Physics*, 63rd edn, p. 27. CRC Press, Boca Raton, Fla (1982).